The interface study of photoresist/underlayer using hybrid x-ray reflectivity and x-ray standing wave approach

Atul Tiwari[1], Roberto Fallica[2], Marcelo D. Ackermann[1], Igor A. Makhotkin[1*]
1 Industrial Focus Group XUV Optics, MESA+ Institute for Nanotechnology, University of Twente, Drienerlolaan 5, 7522 NB Enschede, The Netherlands; 2 IMEC, Kapeldreef 75, 3001 Leuven, Belgium

ABSTRACT

We have studied the gradient of photoacid generator (PAG) concentration across the photoresist (PR) layer. The pristine and after exposure to Extreme ultraviolet (EUV) PR layers were characterized. The model resist employed in this study was a chemically amplified resist (CAR) containing sulfur (S) as part of the PAG. The geometrical information about PR layers and element profiles was obtained by applying a hybrid x-ray reflectivity (XRR) and X-ray standing wave (XSW) data analysis using x-ray using a laboratory Cu Kα1 source. The information about S-profile was retrieved from the combined analysis of angular-dependent XRF measurements of S (the XSW data) and XRR data. We have shown that the XSW technique may efficiently be used for analyses of the geometrical parameters of PR layers and underlayers and for retrieving profiles of S concentration.

Keywords: Hybrid X-ray metrology, Photoresist study, X-ray reflectivity, X-ray Standing Waves.

1. INTRODUCTION

Extreme ultraviolet lithography (EUVL) is a cutting-edge technology that utilizes EUV light to create fine patterns for fabrication of microelectronic devices. The photoresist plays an important role in this lithography process. The chemically amplified resist's (CARs) are a type of PR which was found to increase the sensitivity of the lithography process to create fine patterns [1, 2]. This type of resist consists of three main components, i) polymer, ii) base quencher and iii) photoacid generator (PAG). The PAG is a key element that generates acid upon EUV exposure. This acid creates chemical change in the polymer to make it soluble in a developer solution. The role of the quencher is to prevent unwanted reactions before exposure by controlling the reactivity of the photoacid.

Several efforts have been made to be in line with Moore's law for example photoresist thickness optimization [3, 4], underlayer material and its thickness optimization [5, 6], PR formulation [7], sensitivity enhancement [2], resist outgassing [8] to name a few. The research is still ongoing to gain fundamental understanding about the chemistry of the polymer, quencher and PAG, and a few questions still remain unclear. For example, the distribution of PAG in the photoresist film [9] and the interaction between photoresist and underlayer [10]. The distribution of PAG affects the uniformity of acid generation during exposure, influencing the quality and precision of the pattern transfer in the fabrication process. The interaction between photoresist and underlayer is important for optimizing adhesion and preventing issues like delamination and ensuring the reliability of devices. Recent study of the secondary-ion mass spectroscopy (SIMS) analysis on thin EUV photoresist by Spampinato et. al. focusses on the photo-induced fragmentation of PAG molecule with an application of application of GCIB-SIMS technique [11]. The Orbitrap™ SIMS approach was able to verify the presence of a PAG-related molecule which was not possible with the traditional ToF-SIMS technique.

In the current work, the hybrid XRR and XSW approach has been used i) to study the possibility of analysing the distribution of PAG across blanket PR, and ii) to examine its migration towards the underlayer/substrate. The PAG in the PR samples used in this study is a sulfur-containing PAG. Tracing S in the PAG by measuring S fluorescence as a function of incidence angle modulated by XSW formed in total external reflection mode can be helpful in achieving these objectives. The first results and their interpretation are presented in this paper.

*i.makhotkin@utwente.nl

Metrology, Inspection, and Process Control XXXVIII, edited by Matthew J. Sendelbach,
Nivea G. Schuch, Proc. of SPIE Vol. 12955, 1295505 · © 2024 SPIE
0277-786X · doi: 10.1117/12.3010917

2. MATERIALS AND METHODS

The sample discussed here was prepared by spin coating of an organic chemically amplified PR designed for EUV lithography on a substrate. The substrate was bulk a crystalline silicon (Si) which had been pre-treated with diluted HF to remove its native oxide. The thickness of the PR layer was 35 nm. The PR consists of a polymer matrix that contains protecting groups that are cleaved during EUV exposure by the photoacid; the rest of the photoresist is blended with a smaller percentage of PAG and quencher. Importantly, only the PAG (triphenylsulphonium) contains S atoms. One piece was exposed to EUV radiation equal to its dose-to-clear (which is the amount of light needed to trigger the photoacid generation and deprotection of the polymer chain), while another piece was kept unexposed to compare the S atomic distribution before and after EUV exposure.

The samples were first characterized by extended XRR using Malvern PANalytical EMPYREAN X-ray diffractometer equipped with a monochromatized Cu-Kα1 (1.54 Å) x-ray source. The reflectivity measurement from 0.1º – 3º was completed in 4 h, in three angular segments from 0.1º – 0.7º, 0.7º – 1.4º, and 1.4º – 3.0º with a step size of 0.005º. This allowed to resolve Kiessig fringes at higher angles by measuring for a longer time. To collect XRF data, an AMPTEK detector with 128 eV energy resolution was used. The fluorescence signal modulated by XSW was recorded in the angular range from 0.0º – 0.8º with step size and acquisition time of 0.005º and 30 s, respectively. To retrieve the XRF signal of S as a function of the incidence angle, the XRF spectra were analyzed using the PyMca program [12]. The XRR and XRF measurements were done in a single run without removing the sample from the sample stage.

The XSW were formed above the substrate in total external reflection mode. As the angle of incidence increases from zero towards the critical angle of silicon (Si), the position of antinodes as well their periodicity changes. The fluorescence of S by modulated XSW contains information about the distribution of S in the analyzed film. On the other hand, the XRR curve holds information about the electron density profile of the analyzed film. The analysis of these samples by a single technique (either XRR or XRF) is complicated because of the low contrast between the analyzed layers (PR and organic underlayer). Whereas the combined method using the same model to analyze XRR and XRF data sets should yield more reliable results compared to each individual measurement.

In this work the XRR and XRF data were analyzed using a hybrid free-form approach similar to that described in [13]. The analysis of XRR and XRF data results in the determination of the δ profile and the elemental distribution, where $1-\delta$ is the real part of the refractive index. The δ profile provides information about the optical constants of the material in the sample. The elemental distribution illustrates how each element is spatially distributed within the sample. The combined analysis allowed us to reduce the cross-correlations between the model parameters during the analysis of XRR by adding XRF data set that is sensitive to the phase of the reflected waves. This approach partially solves the well-known phase problem of XRR.

Given that the PR is sensitive to light, prolonged exposure could alter its structure or thickness. As a precaution, it is essential to determine the stability of the PR film under long-term exposure to Cu-Kα1 (1.54 Å) x-ray source. To assess this, several XRR reflectivity measurements were performed over a total duration of 15 hours. The observations did not reveal any significant changes of the film thickness, suggesting that Cu-Kα1 radiation is suitable for characterizing PR films in a laboratory setting.

3. RESULTS AND DISCUSSION

Upon qualitatively comparing XRR and XRF datasets from unexposed and exposed states, a change in the oscillation period of the XRR pattern and a shift of the S fluorescence peak were observed. The change in the XRR oscillation period after exposure can be attributed to a decrease in the PR film thickness. The shift of the S fluorescence peak after exposure can be attributed to the possible redistribution of S. The XRR and XRF datasets of the unexposed and exposed states were fitted using a free-form approach, resulting in a good agreement between the experimental and fitted data. Figures 1(a) and 1(b) compare the δ profiles and distributions of S across the PR film thickness in its unexposed and exposed states. The PR film thickness in the unexposed state was found to be ~32.3 nm, calculated from the FWHM of the S distribution in the unexposed state. After exposure, an increase of ~8% in the δ value and a decrease of ~2.1 nm in the PR film thickness were observed, as shown in Figures 1(a) and 1(b), respectively.

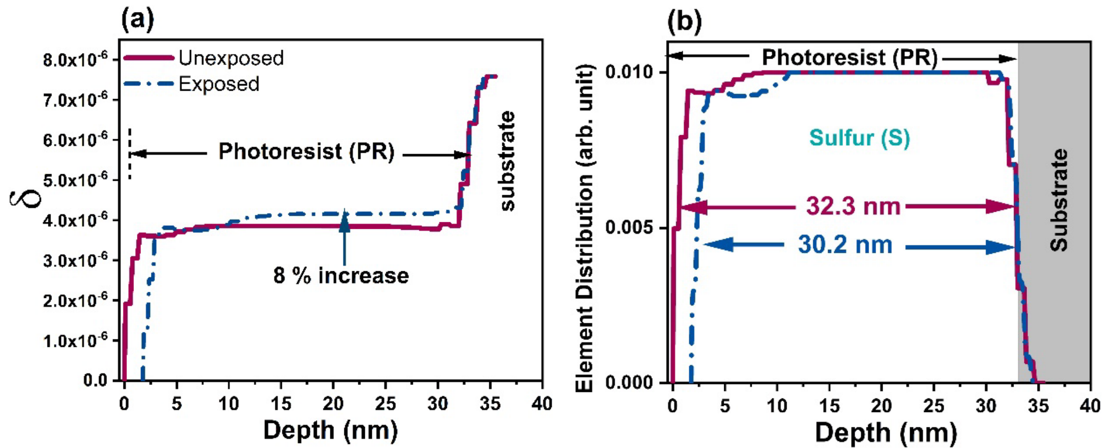

Figure 1. (a) δ profile and (b) distribution of S across the PR film thickness before and after exposure.

The hybrid XRR-XSW analysis indicated the decrease in the photoresist (PR) layer thickness and an increase in the δ value of PR after exposure. The δ value rise could be linked to S redistribution or indirectly to chemical transformations in the S-containing PAG due to exposure. The distribution of PAG in the PR layer was observed to be homogeneous across the PR thickness.

Though amount of S in the PR layer is expected to be very low, we can conclude that laboratory X-ray setup has enough beam intensity to record high-quality XSW data from S. The sensitivity of standing waves formed below the Si critical angle of 0.2 degrees in total external reflection region is limited by the large standing wave period. The standing wave period below the critical angle of Si is approximately 59 nm which is larger than the thickness of the PR layer. In future work, to improve the sensitivity of XSW to the changes at interfaces, the XSW-modulating layer will be deposited beneath the PR layer such that the standing wave period modulation will be comparable to the expected changes in the EUV-induced S distributions.

4. CONCLUSIONS

Here we have shown preliminary experiments regarding the applicability of a hybrid XRR and XSW approach for the characterization of EUV-induced structural changes in PR. This analysis was performed both before and after EUV exposure to investigate the feasibility of analyzing the redistribution of the photoacid generator (PAG) within the PR film. Notably, there were minor or no changes in the PR film thickness after 15 hours of exposure, making the Cu-Kα1 source suitable for such characterization.

The distribution of PAG within the PR film was determined by measuring the angular-dependent fluorescence of S, present in PAG. This distribution was found to be homogeneous.

ACKNOWLEDGEMENTS

The work was performed in the frame of the NEXT3D project funded by TKI Connecting Industry call with the support of Malvern Panalytical. We kindly acknowledge S. Yakunin for friendly discussion on XSW technique. We kindly acknowledge the help of Hironori Oka and Keita Kato (Fujifilm Electronic Materials Europe) for providing photoresist materials. We kindly acknowledge Milen Gateshki (Malvern Panalytical) for useful discussions and help with editing of this manuscript.

REFERENCES

[1] I. Junarsa, M.P. Stoykovich, P.F. Nealey, Y. Ma, F. Cerrina, H.H. Solak, Hydrogen silsesquioxane as a high resolution negative-tone resist for extreme ultraviolet lithography, Journal of Vacuum Science & Technology B: Microelectronics and Nanometer Structures Processing, Measurement, and Phenomena, 23 (2005) 138-143.

[2] T. Kozawa, S. Tagawa, Radiation Chemistry in Chemically Amplified Resists, Japanese Journal of Applied Physics, 49 (2010).
[3] D.D. Simone, A.-M. Goethalss, F.V. Roey, T. Zheng, P. Foubert, E. Hendrickx, G. Vandenberghe, K. Ronse, Progress and Challenges of EUV Lithography Materials, Journal of photopolymer science and technology, 27 (2014) 601-610.
[4] G. Conti, H.P. Martins, I.A. Cordova, J. Ma, R.J. Wojtecki, P. Nalleau, S. Nemsak, Chemical and structural characteriation of EUV potoresist as a function of depth by standing wave x-ray photoelectron spectroscopy, J Micro/nanopattern. mater. metrol, 20(3) (2021) 034603-034601 - 034603-034607.
[5] P. Vanelderen, D.D. Simone, V. Spampinato, A. Franquet, G. Vandenberghe, The role of underlayers in EUVL, journal of polymer science and technology, 31 (2018) 209-214.
[6] C.L. Henderson, H. Xu, J.M. Blackwell, T.R. Younkin, K. Min, Underlayer designs to enhance the performance of EUV resists, Advances in Resist Materials and Processing Technology XXVI, 2009.
[7] C.L. Lay, C.S.L. Koh, Y.H. Lee, G.C. Phan-Quang, H.Y.F. Sim, S.X. Leong, X. Han, I.Y. Phang, X.Y. Ling, Two-Photon-Assisted Polymerization and Reduction: Emerging Formulations and Applications, ACS Appl Mater Interfaces, 12 (2020) 10061-10079.
[8] H. Tsubaki, S. Tarutani, N. Inoue, H. Takizawa, T. Goto, EUV resist materials design for 15 nm half pitch and below, journal of polymer science and technology, 5 (2013) 649-657.
[9] Q. Lin, M. Toukhy, M. Paunescu, C. Chen, G. Pawlowski, PAG distribution and acid thermal diffusion study in ultra-thick chemically amplified resist films, Advances in Resist Materials and Processing Technology XXIV, 2007.
[10] S.A. George, B.M. La Fontaine, P.P. Naulleau, A. Krishnamoorthy, Z. Wu, J.E.W. Rutter, J.T. Kennedy, S.Y. Xie, K.Y. Flanigan, T.I. Wallow, Characterization of line-edge roughness (LER) propagation from resists: underlayer interfaces in ultrathin resist films, Extreme Ultraviolet (EUV) Lithography, 2010.
[11] V. Spampinato, A. Franquet, D. De Simone, I. Pollentier, A. Pirkl, H. Oka, P. van der Heide, SIMS Analysis of Thin EUV Photoresist Films, Anal Chem, 94 (2022) 2408-2415.
[12] V.A. Solé, E. Papillon, M. Cotte, P. Walter, J. Susini, A multiplatform code for the analysis of energy-dispersive X-ray fluorescence spectra, Spectrochimica Acta Part B: Atomic Spectroscopy, 62 (2007) 63-68.
[13] O.A. Kondratev, I.A. Makhotkin, S.N. Yakunin, Atomic separation in Co/Cu/Co magnetic structures study by hybrid X-ray reflectivity – X-ray standing wave approach, Applied Surface Science, 574 (2022).